

# Slope stability assessment of an open pit mine using three-dimensional rock mass modeling

Mario Morales<sup>1</sup>  · K. K. Panthi<sup>1</sup> · K. Botsialas<sup>2</sup>

Received: 5 April 2017 / Accepted: 5 October 2017 / Published online: 23 October 2017  
© Springer-Verlag GmbH Germany 2017

**Abstract** Rock mass classification systems are commonly used to evaluate the likelihood of instability in mining environments. Most frequently used classification systems are the rock mass rating (RMR), geological strength index (GSI), and the Q-system. These methods are used widespread among geotechnical engineers as one practical way to assess quality of the rock mass. In most hard rock open pit mines, bench faces with no clear discontinuities present one or two joint sets that may dominate on the failure mechanism. To address this, slope mass rating (SMR), which is a modified version of the RMR system of rock mass classification, can be used. The benefit is that SMR takes into consideration the influence of joint orientation on the classification method itself. Hence, the main aim of this paper is: first, to develop a three-dimensional RMR model of an open pit mine under active operation based on the extensive field mapping carried out, and then produce an SMR surface model that is derived using current topography, modeled RMR values and jointing conditions prevailing in each structural domain. The final goal is to create an SMR susceptibility map of the mine area for the dominant topographic condition and the main structural domains present in the open pit, and to present a methodology that may be easily replicated at any given hard rock open pit mine. The authors emphasize that the use of an SMR model is a very helpful tool in evaluating the areas of the mine that are most vulnerable to

potential slope instability in different periods of operation of the mine.

**Keywords** Slope stability · Rock mechanics · Rock mass model · Mining slope · Mining geotechnics

## Introduction

Open pit mining excavates the earth surface in order to reach the underlying valuable ore. Planning of an open pit is a matter of determining the most profitable pit limit and the most economical mining sequence for a given mineralization (Steffen 1970). During the exploitation phase, the excavation sequence implies the development of artificial slopes on which stability is a crucial factor both for safety and financial viability of the mining. Therefore, the stability assessment of an open pit rock slope is an essential requirement of the open pit mine not only during the feasibility and detail design studies but also throughout the operational life of the project. Rock mass classification systems are extensively and often used to quantitatively classify the quality of the exposed rock mass in the open pit slopes. There are varieties of rock mass classification systems that have been proposed in the last 50 years. Four of these classification systems have gained broad acceptance in the mining industry, which are the rock mass rating (RMR) of Bieniawski (1973), the Norwegian Q-system (Barton et al. 1974), the MRMR (also known as Laubscher's RMR) updated by Laubscher (1990), and the geological strength index (GSI) system proposed by Hoek (1994) and later modified by Marinos and Hoek (2000). Flores and Karzulovic (2002) described that the most used method of rock mass classification in underground mines is MRMR, which accounts for 53%, followed by the Q-system (26%) and the RMR system (15%). On the other hand, the most used method of rock mass

---

✉ Mario Morales  
mario.morales@ntnu.no

<sup>1</sup> Norwegian University of Science and Technology (NTNU), Trondheim, Norway

<sup>2</sup> Mining Company, AS, Trondheim, Norway

classification in open pit mining is Hoek's GSI (39%), followed by RMR (26%) and MRMR (22%). The disadvantages and limitations of rock mass classification systems with respect to stability assessment of slopes have been discussed in detail by Pantelidis (2009).

In addition to the above-mentioned methods of rock mass classification systems, the slope mass rating (SMR), which is an adjusted version of the RMR and was proposed by Romana (1985), has gained acceptance in recent years, especially for pit slope and cut slope stability assessments. According to Aksoy (2008), the direct application of RMR for slopes may in some cases give meaningless results. The SMR is a rock mass rating tool for risk-based evaluation of slope instability at a particular slope face and its relation with discontinuities prevailing in the rock mass. The SMR adjusts RMR values by accounting for four more factors as explained by Eq. 1 (Romana 1985).

$$SMR = RMR - (F1 \cdot F2 \cdot F3) + F4 \quad (1)$$

The product of three factors (F1, F2 and F3) is an adjustment rating directly related to the discontinuity systems prevailing in the rock slope. The first factor (F1) accounts for the parallelism of the strikes of the discontinuities and the slope face, the second factor (F2) for the dipping angle of the discontinuities, the third factor (F3) for the relation between the slope face angle and the dip of the discontinuity, and the last factor (F4) accounts for the influence of the quality of blasting (or excavation method) into the slope face. Tomás et al. (2007) proposed an alternative way that was originally proposed by Romana (1985, 1993) to calculate the first three factors of the SMR based on the continuous functions. The authors demonstrated that these functions show maximum absolute difference with discrete functions lower than seven points.

Many authors have applied geostatistics to investigate fracture distribution in a rock mass (Long and Billaux 1987; Chilès 1988; Rafiee and Vinches 2008) and to estimate different rock mass properties (Yu and Mostyn 1993; Ellefmo and Eidsvik 2009). Similarly, the interpolation of areas of same RMR level based on point observations in the field has been proposed as a suitable method to extend the point ratings to a surface by Öztürk (2002) and Ryu et al. (2003). Ferrari et al. (2014) revealed that the resulting RMR map based on spatial estimation by geostatistical analysis can be a useful tool to estimate the quality of outcropping rock mass and to assess the geotechnical behavior of the mapped area. The RMR index has been assessed using geostatistical analysis since early 2000, especially for underground projects. The kriging method is extensively used for both borehole and surface datasets. RMR values have always been considered as a single regionalized variable (Stavropoulou et al. 2007 and; Exadaktylos and Stavropoulou 2008), and also as the sum of many variables (Egaña and Ortiz 2013). The Q-system is estimated as a

single variable by geostatistical methods analyzing its effects on tunnel boring machine-related parameters (Exadaktylos et al. 2008). However, one should note that there are limitations in each classification system, as discussed by Palmstrom and Broch (2006) and Marinos et al. (2005). If carefully used, these classification systems can provide very useful information on slope stability during planning and design stages as well as during construction and operation phases. In addition, classification systems can also be used to assess the properties of the rock mass in a very systematic and standardized way (Hoek 2006).

This manuscript tries first to interlink and compare the rock mass quality class assigned using three different classification systems (RMR, Q and GSI) aiming to develop a three-dimensional (3D) rock mass model of an open pit mine located in Norway based on the RMR rock mass classification system. The manuscript further assesses possible unstable areas in the open pit mine slope by adjusting the RMR values to SMR values combining the mine topography with detailed information of slope orientation, slope angle and main jointing orientations achieved from the 3D structural model developed by Morales et al. (2017). Development of such SMR surface model is helpful to reveal large-scale and bench-scale potential movements in the pit slope, which are critical components for risk management practices in slope stability, similar to that discussed by Panthi and Nilsen (2006). Due to sensitivity, no detailed information of the ore body, including location of the mine, will be provided in the manuscript, which has no implication on the research outcome of this manuscript.

### Brief about the open pit mine case

The open pit mine has been in operation over 60 years now and is currently one of the major hard-rock deposits of its kind. The geometry of the slope is defined by a first pass to define an initial single bench height of 15 m, which is doubled in the second pass to have an overall height of 30 m. Therefore, the overall slope angle of the mine is between 45 and 55°. The open pit has a length of approximately 3 km and the current depth is close to 240 m from the top. The mining activity is planned to continue for many years to come and will extend the depth of the pit significantly from what it is at present. Therefore, the short-, medium- and long-term stability are crucial issues for this mine.

### Geology

The area is characterized by a great anorthosite intrusion into which the ore body is intruded. The structure of the ore becomes increasingly complex in the east. Xenoliths of anorthosite are present within the ore body. The anorthosite, which is located within the ore body or in the contact zones of the ore

body, typically shows more alteration than in the surrounding rock mass of the pit slope. Two major diabase dikes crosscut the ore body in a WNW-ESE direction. These dikes have a straight appearance and dip almost vertically. The largest main dike (furthest to the south) is about 25 m wide (Fig. 1). As the main dike exits the ore body in the east, it forms a swarm of several smaller dikes extending from the main body. Several studies have shown that there are some areas of heavy alteration that are related to fractures and fault systems at the mine site, on both the ore body and anorthosite.

### Structural domains

Morales et al. (2017) have shown that there are six different regional lineaments, which are correlated with the regional pattern of discontinuities. In this manner, it was also possible to distinguish six different fracture systems (FS) in the mine area. Based on the jointing associated with each of these FS, a total of eight structural domains were identified and a 3D structural model was presented. Structural domains are, in general, not concretely defined (Read and Stacey 2009) with a fixed boundary between them, but rather created in such a way that overlapping is possible to better interpret the transition between structural domains.

These structural domains are associated with one or more FS; an example is the case of structural domain 08, which is associated with FS6 in the upper portion of the hanging wall (HW) in the northwestern part of the mine. The structural domains can be seen in Fig. 1, while Table 1 summarizes the structural domains and major joint sets associated with different FS.

## Methodology

The development of the rock mass model is based in two sources of information; i.e. the surface mapping of the mine that assigns RMR, Q and GSI values to the mapped zone and the underground mapping, which is achieved through the inspection and analysis of boreholes and mapping of drainage tunnels. The surface mapping provides a bi-dimensional interpretation of the distribution of the quality, which at some extent is close to 3D since the mapping is done in m-benches at different z-coordinates. On the other hand, the borehole offers information about a specific point along the axis that could be extrapolated to two or three dimensions when combined with other boreholes in the neighborhood. Therefore, these two layers are combined in order to build the most accurate 3D interpretation of the quality of the rock mass in the mine area.

The method begins with data acquisition, in which field mapping is done in selected positions along the open pit, inside the drainage tunnels and core logging. Collected individual parameters are associated with estimate RMR and Q values. In addition, GSI values were estimated based on the visual inspection of the slope. After the data

was collected, validation was carried out and comparison between RMR and GSI against Q was made in order to verify if the rock mass classifications assigned to each one are in line with the typical relationships proposed by Bieniawski (1989) and Hoek (1997). This may not indicate whether the rating is well-assigned since rock mass classifications are highly subjective and relative to the one involved in the mapping. However, it is for certain that it will provide a sound basis for evaluating equal criteria when assessing different methods. These first two steps are the ones necessary to create a sound database for further work.

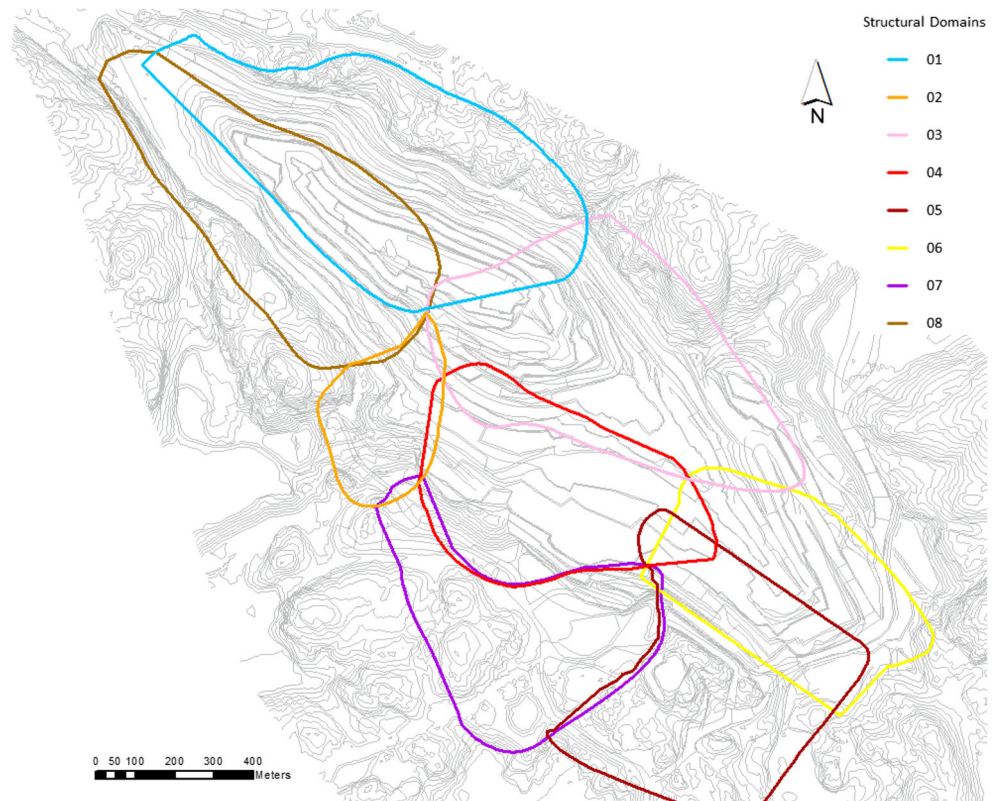
Once the database was generated, preliminary surfaces maps for RMR, GSI and Q distribution were interpolated into geographical information system (GIS) software. The parameters were set to RMR values and calculated accordingly to GSI and Q. For validation of these parameters, the database was split into two subsets: modeling and control. Furthermore, 80% of the data were kept on the part of the modeling subset, while the remaining 20% were kept for quality control. The ratio of 80% and 20% was successfully used by Egaña and Ortiz (2013) in the validation of RMR values. This procedure is repeated 5 times with 5 randomly generated datasets following the 80/20 rule in order to quantify the error. The result of this stage is the preliminary contours and isocurves based in certain threshold values were extracted from the map. Each threshold was selected based on the typical quality class range. The contours were also smoothed in order to avoid peaks or strange geometries in the final output.

In parallel, an assessment of RMR values in boreholes was done. As the purpose of the research is to produce an SMR model, the quality assessment of the rock mass from boreholes was carried out using RMR. Low-RMR zones were identified and correlated with the structural model of the mine developed by Morales et al. (2017). The structures that influenced in lowering RMR values in the boreholes and estimated by field mapping were added to the preliminary contours. Finally, surface contours of RMR values were developed by considering discontinuity structures affecting the quality of the rock mass and were added to the ArcGIS model.

Further, based on the RMR data from boreholes, a preliminary 3D RMR model was developed. The outcome of this step does not necessarily have to match the final surface contouring of the RMR values. Hence, the 3D model was later adjusted with the surface information from the final contours and incorporated into the model to match the RMR values mapped at the surface. The output was the final 3D distribution of RMR describing the 3D rock mass quality model.

After creation of the 3D rock mass quality model based on RMR, SMR values were calculated in the pit surface taking in account the finalized RMR values, the dip and

**Fig. 1** Map of the mine area with structural domains (modified from Morales et al. 2017)



the dip direction from the slope face and the jointing information. The information on jointing was traced from the already established structural domains of the mine by Morales et al. (2017). The SMR map was developed for both the total slope and for the slope in bench scale. This is necessary to assess scale effect on the potential instability condition of the pit slope for short-term, medium-term and long-term and also to verify the correctness of our assessment with the areas potentially prone to instabilities. A diagram illustrating how steps are performed in order to create the model is presented in Fig. 2.

**Table 1** Structural domains with jointing direction and associated fracture systems in the mine area (modified from Morales et al. 2017)

Structural domain	Joint set			Associated FS		
	J1	J2	J3	J1	J2	J3
01	89/029	89/268	–	FS5	FS1	–
02	77/269	63/346	–	FS1	FS3	–
03	84/314	78/218	76/025	FS2	FS5	FS4
04	43/051	56/356	75/219	FS6	FS3	FS5
05	85/040	–	–	FS4	–	–
06	78/272	81/239	82/216	FS1	FS5	FS4
07	84/128	–	–	FS2	–	–
08	49/054	–	–	FS6	–	–

## Field work and data acquisition

Data gathering and correct interpretation is extremely important since quality of accumulated data sources are mainly responsible for the quality of the end model. Some of the important steps of data acquisition were as follows:

- Study on regional geology, regional faulting, main lineaments and placement of the ore body is very important and has a close relationship with the different lithological and structural domains in the mine pit.
- Structural mapping of the different domains and rock types control both bench design and overall stability. This includes both joint sets as well as major features such as dykes, faults, contacts, etc.
- Identification of alteration zones within the pit is important. Alteration affects rock strength; therefore, different alterations within the same rock type were grouped separately.
- Laboratory testing of different rock types with the results grouped by alteration for each rock type.

## Surface mapping

The surface mapping was done in the summer months of years 2015 and 2016. It consisted mainly of performing the following five steps at every location:

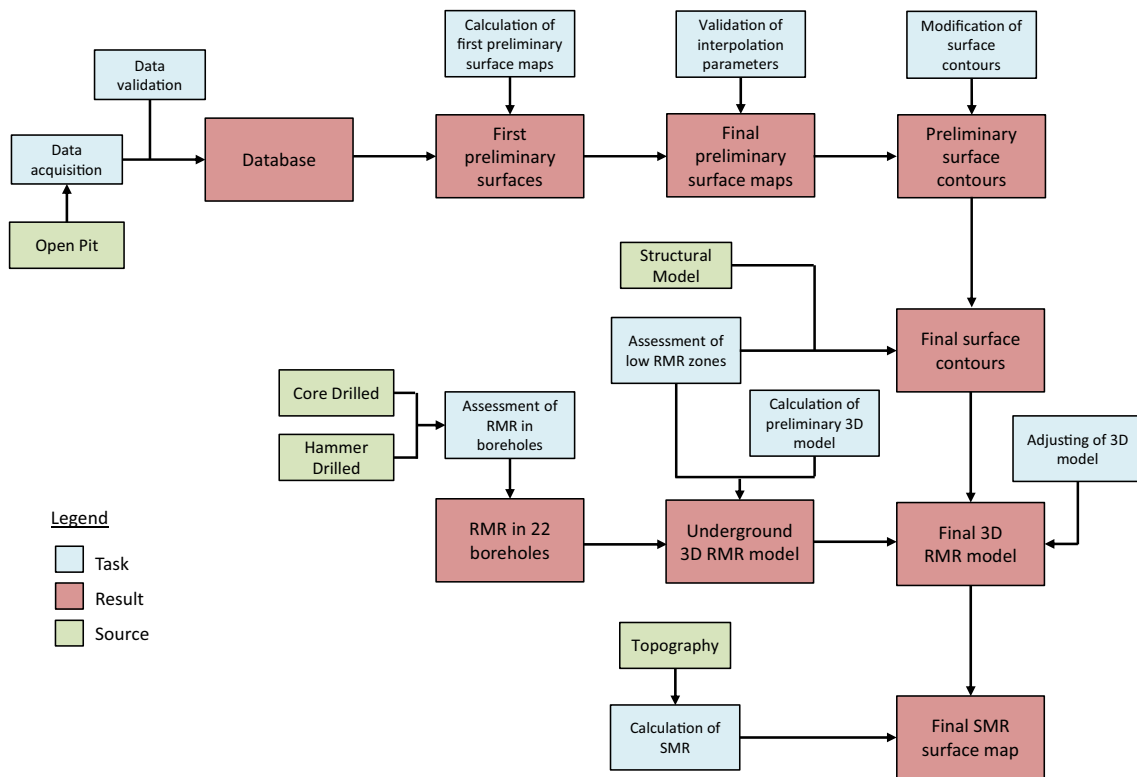


Fig. 2 Flowchart for the calculation of surface SMR maps based on topography and 3D RMR distribution

1. Measuring orientation (dip/dip direction) for each joint set that was possible to access.
2. Schmidt hammer testing of the most unfavorable exposed joint surface.
3. Assessment of RMR parameters.
4. Assessment of Q parameters.
5. Estimation of GSI value.

The mapping covered most of the mine area that was accessible during the field work period. A total of 197 surface points were logged. The distribution of the mapping locations is shown in the Fig. 3. The figure also shows the location of drill holes (core drill and hammer drill holes).

In order to assess the reliability of the rating assigned in the field, RMR, GSI and Q ratings were compared. In this aspect, it is well known from Bieniawski (1989) and Hoek (1997) that there are two relationships between RMR and Q and GSI:

$$RMR = 9 \cdot \ln(Q) + 44 \tag{2}$$

$$RMR = GSI + 5 \tag{3}$$

Combining (2) and (3) gives:

$$GSI = 9 \cdot \ln(Q) + 49 \tag{4}$$

The measurements for RMR and GSI were plotted against the Q value in order to establish if they follow (or not) the

relationships given above. The resulting graph (Fig. 4) shows that the best fits for each dataset are approximately as follows:

$$RMR = 8 \cdot \ln(Q) + 53 \tag{5}$$

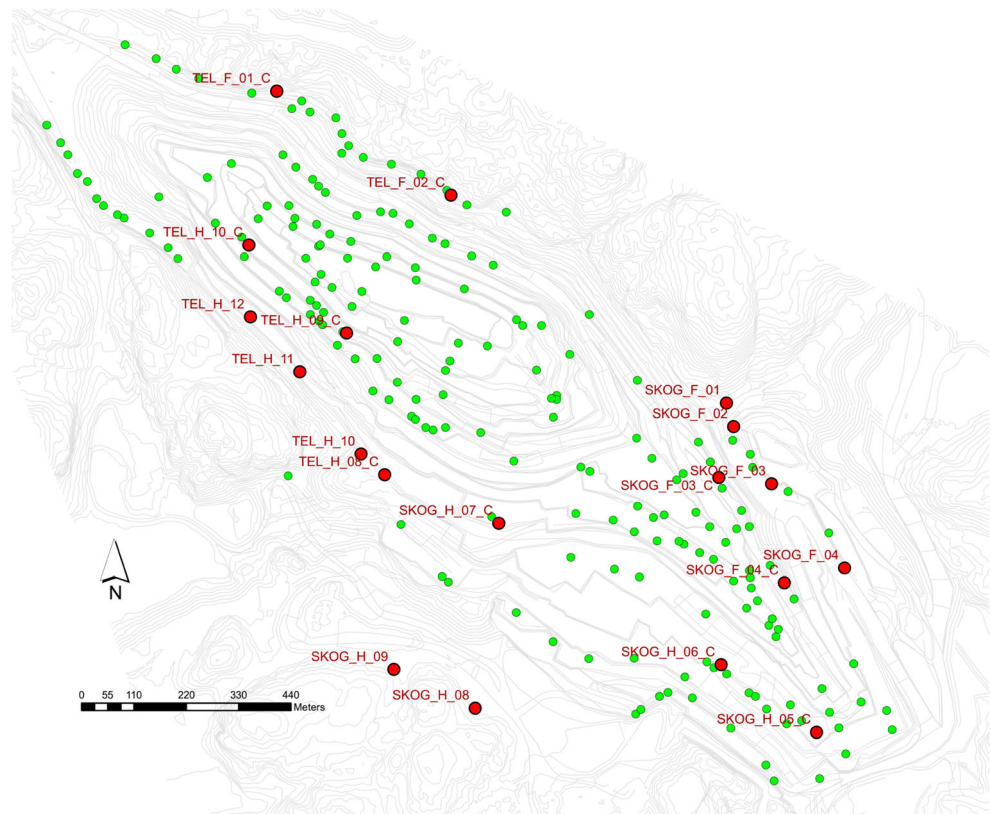
$$GSI = 8 \cdot \ln(Q) + 48 \tag{6}$$

Combining Eqs. 5 and 6 will give results similar to those expressed by Eq. 3 suggesting that the correlation achieved through the mapping results are valid to interpolate from one rock mass classification to the other, which increased the reliability level of the classification achieved through field mapping.

### Underground mapping

Interpreting an RMR based on information from boreholes is not a straightforward process, since it requires many assumptions and generalizations in order to assign correct and prudent values. The project has a total of 22 boreholes (Fig. 3). 10 of them were core-drilled and manually logged in 2015 and 2016. The remaining 12 holes were hammer-drilled, and the available information was through geophysical logging. Different assumptions were made for each of the two sets of boreholes, since the information coming from both is not equal.

**Fig. 3** Distribution of surface mapping locations (green dots) along the mine



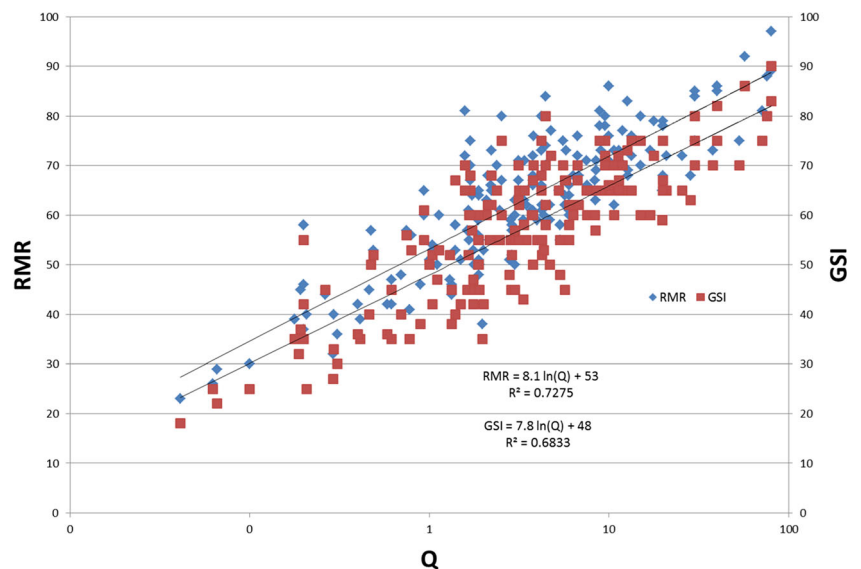
*Core-drilled boreholes*

Core-drilled boreholes were logged every 1 m of core length registering rock quality designation (RQD), total core recovery (TCR), solid core recovery (SCR), frequency of fractures per meter (FFm), number of joint sets, weathering index, and strength index. Also, for each open fracture, the roughness index (JRC), alteration number (Ja), approximated basic friction angle, and the weathering of filling material were

recorded. Closed fractures were also registered in position. In order to calculate the RMR, the parameters were derived based on the following:

1. Uniaxial compressive strength (UCS): the rating was assigned from the UCS obtained for samples coming from the different lithologies in the area, and tested in the laboratory. Each segment of the borehole length has an associated lithology.

**Fig. 4** Comparison of RMR and GSI ratings against Q value



2. RQD: obtained directly from the core logging.
  3. Spacing of discontinuities: based on the total number of joint sets and FFm. If there are no joints, then it was assumed to be more than 1 m.
  4. Condition of discontinuities
    - a) Length, persistence: not possible to obtain directly. It was assigned a common value based on 15-m persistence, since it is the height of benches in the mine.
    - b) Aperture: obtained directly from the core logging.
    - c) Smoothness: JRC directly measured in the core logging and it was transformed into RMR following Table 2.
    - d) Infilling: derived from the alteration number Ja, assessed directly from the core.
    - e) Alteration/weathering: assessed directly from the exposed open joint walls.
  5. Groundwater conditions: not possible to obtain, the rating has been assumed as wet.
4. Condition of discontinuities
    - f) Length, persistence: not possible to obtain directly. It was assigned a common value based in 15-m persistence, same as to the core-drilled boreholes.
    - g) Aperture: obtained directly from the core logging.
    - h) Smoothness: A surface mapping campaign for recording values of dip, dip direction, JRC and amplitude (in a 10-cm, 20-cm and 1-m scale) was carried out in the summer of 2016. The values were then analyzed to find a correlation between the roughness rating assigned via the RMR and the dip/dip direction. The results of the investigation are shown in Table 3. JRC values were transformed into ratings following the ratings shown in Table 2.
    - i) Infilling: it was calculated from the potassium and thorium content. Geophysical logging was performed inside the hammer-drilled boreholes. Part of the logging was conducted with a spectral gamma sonde, which measures energy levels with respect to the different radioactive elements. The calculated curves of K-40, uranium and thorium concentrations were assessed, and the anomalies of potassium and thorium against depth were used in order to define the presence of clayey minerals
    - j) Alteration/weathering: it was derived from the potassium and thorium content, since there is a correlation to the presence of alteration zones.
  5. Groundwater conditions: Flowmeter tests along with hydraulic tests, such as slug tests and, double- and single-packer tests, were used in order to derive the fractures that are water-bearing. The RMR was based on the results of these tests and the estimation of flow. A rating of 7 is assumed for the rest of the boreholes without flow testing, assuming a moderately wet condition.

### Hammer-drilled boreholes

Hammer-drilled boreholes were logged recording data every 5 cm through geophysical inspection with an acoustic televiewer (Riglar et al. 2016). The method is able to register the position of a joint and calculate its aperture, dip and dip direction. Other parameters associated, like estimated content of potassium, are also possible to derive from the results. To calculate the RMR, the ratings were evaluated as following:

1. UCS: same as for the core-drilled boreholes.
2. RQD: calculated from the number of fractures given for a length of 1 m.
3. Spacing of discontinuities: calculated from the position of each fracture. If there are no joints, then it was assumed to be more than 1 m.

**Table 2** RMR assigned to roughness profile (JRC as in Barton and Choubey 1977)

JRC	RMR
0–2	0
2–4	0
4–6	1
6–8	1
8–10	3
10–12	3
12–14	5
14–16	5
16–18	6
18–20	6

## Development of the model

### Preliminary maps and surface validation

RMR, Q and GSI surface maps were developed based on the results from the field mapping. Among diverse kriging methods, You and Lee (2006) and Choi et al. (2009) have used indicator kriging to estimate RMR classes. Since the RMR values of the study area fall within only three classes, the ordinary numerical kriging was selected, as was done by Ferrari et al. (2014), and Exadaktylos and Stavropoulou (2008), instead of indicator kriging. It is highlighted here that the indicator kriging

**Table 3** Average roughness rating and JRC class per fracture system

Fracture system	Amplitude profile rating [cm]			Avg. rating	Avg. JRC	RMR
	10	20	100			
FS1	6.00	5.50	5.00	5.50	16–20	5
FS2	1.41	2.06	2.88	2.12	6–10	2
FS3	5.75	5.50	6.00	5.75	18–20	6
FS4	3.22	3.49	2.65	3.12	8–12	3
FS5	3.92	4.25	3.64	3.94	10–14	4
FS6	3.40	3.55	2.50	3.15	8–12	3

needs an indicator transformation, which continuously needs extra information about significantly high or significantly low values falling within the same class. However, whether a value is slightly larger or much larger than the chosen threshold, in fact, does not play a significant role. Therefore, ordinary kriging was chosen to take into account the entire data set range. An ordinary kriging gives the best linear, unbiased prediction of the intermediate values between two field measurement points. The method uses three parameters for the estimation, which were analyzed and established as follows:

- **Major range:** Represents a distance beyond which there is little or no correlation. Trials were done with 50, 100, 200 and 400 m. The maps represented by 50 and 100 m are not characteristic enough (contradicting with the field experience) of what it is possible to understand in the mine. There is also small difference between 200 and 400 m, and the last one was used as definitive number. Ferrari et al. (2014) noted that in 2D models, the minimum mean error is obtained by performing kriging on the longest lag distance, and he used 1000 m as the range in a regional scale. Hence, it should be understood that the chosen range (400 m) represents fairly good extent considering local scale for this mine.
- **Partial sill:** The difference between the nugget and the sill. A value of 80 was used after trying 50, 70, 80 and 95. It is logical to accept this value as representative since

the highest possible RMR that was mapped in the mine was around 85.

- **Nugget:** Represents the error and variation at spatial scales too fine to detect. The nugget effect is seen as a discontinuity at the origin. Trials were done with 5, 10 and 20, 5 being the value selected.

In every resulting surface map, contours were developed according to rock mass class. The division of the isolines was made following the criteria proposed by Panthi (2006), which is presented in Table 4. As seen in the table, GSI was also added based in Eq. (3).

In order to test the final values, a validation of the model was carried out by splitting the RMR database into two subsets; i.e. the first 80% of the data were used as the modeling subset and the remaining 20% were used as a control set for validation purposes, as was successfully used by Egaña and Ortiz (2013) in validating RMR values. This procedure was repeated 5 times with 5 randomly generated datasets following the 80/20 rule in order to quantify the error. This repetition is necessary to try to isolate errors associated with the occurrence of lower values (i.e. less than 40) as much as possible since values below 40 are not very common and hence may lead to a biased interpretation of the results. Evaluating the control points against the interpolated value gave an average error of 16% compared to the expected value. Since the error is relative to the RMR value in a certain position, the expected

**Table 4** Rock mass classes used for classification (modified from Panthi 2006)

Descriptions		Range of Q values		Range of RMR values		Range of GSI values	
Rock class	Quality	Min.	Max.	Min.	Max.	Min.	Max.
1	Very good to excellent	100	1000	85	100	90	100
2	Good	10	100	65	85	70	90
3	Fair to good	4	10	56	65	61	70
4	Poor	1	4	44	56	49	61
5	Very poor	0.1	1	35	44	40	49
6	Extremely poor	0.01	0.1	20	35	25	40
7	Exceptionally poor	0.001	0.01	5	20	10	25



variation was considered relatively less for low RMR values than for high RMR values. Egaña and Ortiz (2013) reported errors from 7 to 11% in a direct estimation of RMR. Therefore, the parameters used and surfaces achieved were considered as being within acceptable limits. Using relationships between RMR and GSI as well as RMR and Q represented by Eqs. (2) and (3), the parameters were defined following the same criteria for the interpolation of GSI and Q surface maps. The interpolated final maps with 100% data are shown in Fig. 5.

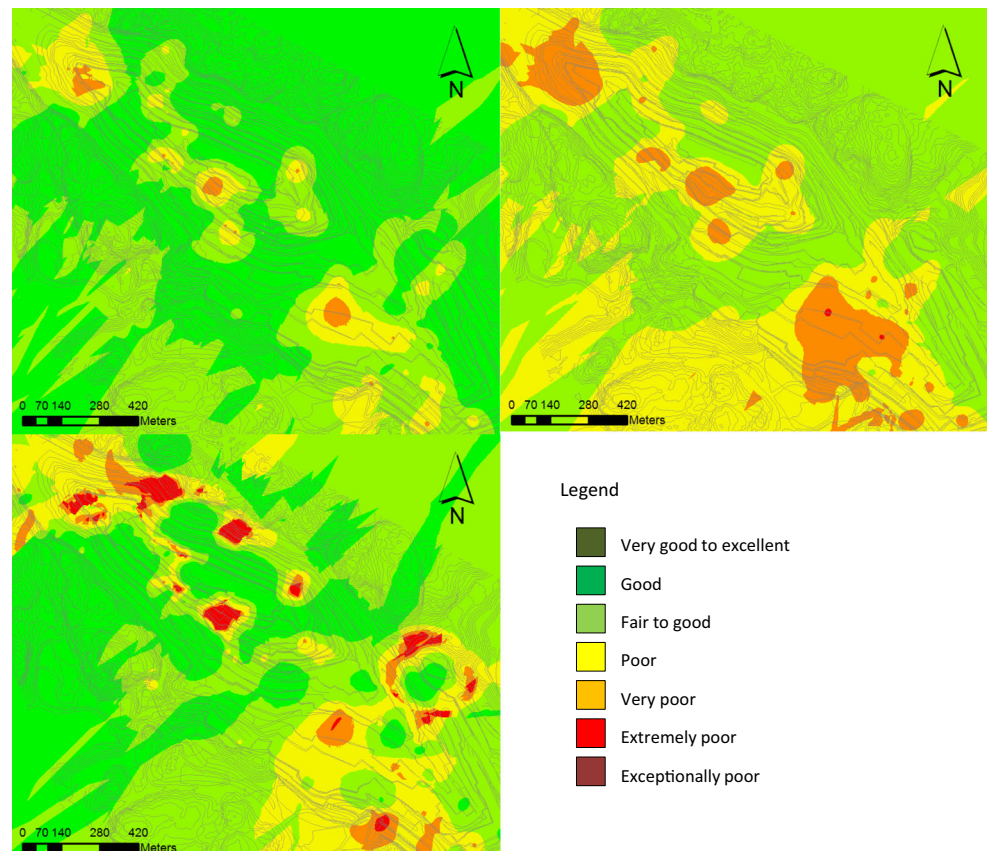
### RMR contours from surface mapping

The resulting contours were modified taking into account the spatial distribution of the field measuring points so that the surface outside the main area of measurements were assigned as “more constant” values. As no measurements were made in the south-western part of the mine that can support the idea of a certain value in that part of the map, contours were smoothed considering better interpretation of what was possible to see in the field. This also applies to the north-east part of the mine. It was interpreted that only contours are rationally defined along the mine, and were adjusted to the most typical values outside (were no data is available). A comparison between the original contours and the smoothed and corrected contours is presented in Fig. 6.

### Correlation between surface maps and borehole RMR

After the surface RMR map was defined, in the next step, attempts were made to make correlations between the mapped values at the surface of the mine and mapped values based on information from the borehole loggings. Low-RMR zones were identified in each borehole according to the same criteria presented in Table 4. After identifying low-RMR zones in each borehole, efforts were placed to analyze RMR values for each interval considering dip and dip direction of the dominant discontinuities. Riglar et al. 2016 has shown that there is a good agreement of the fractures per meter recorded via geophysical and manual logging of the boreholes. Highly fractured zones are very likely to be accurately recorded at the same depth from both methods of logging. Low-RMR zones identified through borehole logging were correlated against the major discontinuity planes mapped in the surface. If consistent agreement between the mapped results from borehole logging and surface mapping were found, then the whole plane was assumed to have influence on the low-RMR zone and the contour was modified accordingly. A total of 19 planes were identified to have agreement, which were intersecting the boreholes at a certain depth. Table 5 shows the interval and the predominant dip and dip direction of the discontinuities compared to surface mapped discontinuities presented in the structural model (Morales et al. 2017).

**Fig. 5** Surface interpolation of RMR (upper left), GSI (upper right) and Q (down left)



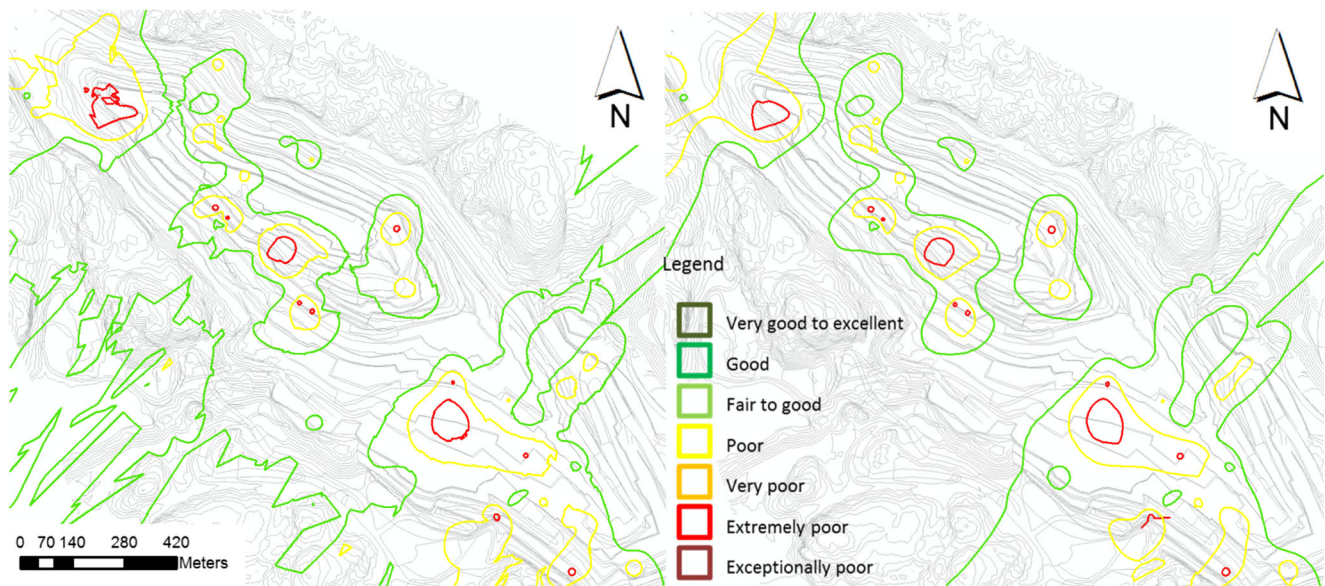


**Fig. 6** Contours for RMR distribution. Left: directly extracted from kriging. Right: smoothed and modified according to actual field conditions

The low-RMR zones were then incorporated into the surface contours with defined new low-RMR zones associated with surface mapping planes shown in Table 5. Modified contours are presented in Fig. 7, which is also the final and modified version of the RMR surface map.

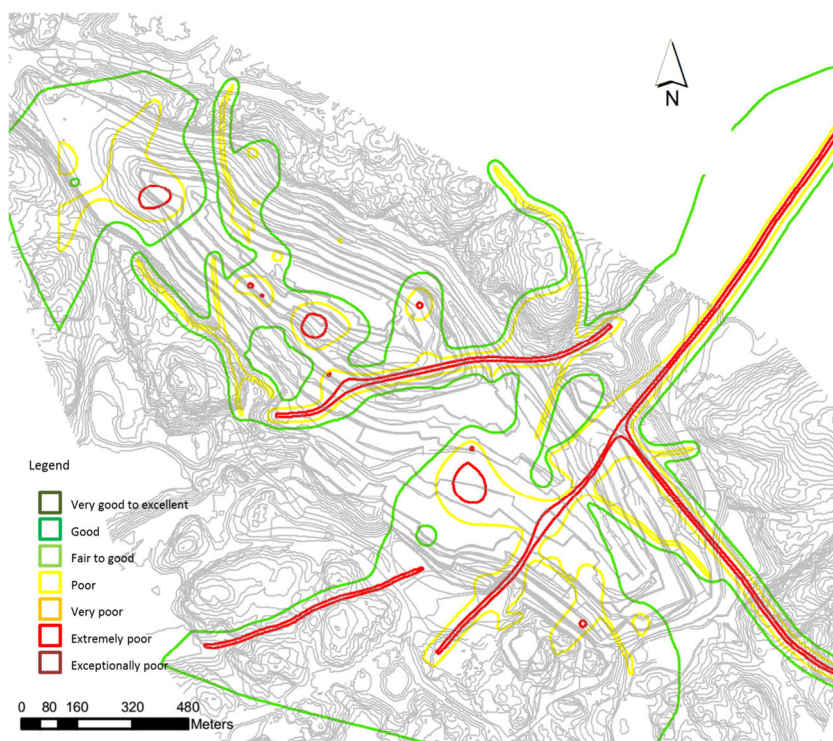
### 3D RMR model

Exploiting the information presented above, a 3D RMR model was developed in Leapfrog Geo software. The main objective of the modeling was to be able to establish a correlation

**Table 5** Low-RMR zones found in boreholes correlated to big planes from structural mapping of mine surface

Borehole	From borehole log					From surface mapping		
	RMR	From	To	Dip	DipDir	RMR	Dip	DipDir
SKOG_F_03_C	70.4	75.4	83	116	76	126		
SKOG_H_06_C	80.5	84.5	63	270	70	290		
TEL_F_01_C	43.6	48.5	76	262	65	232		
TEL_F_01_C	43.6	48.5	72	120	70	118		
SKOG_F_04_C	14.1	50.1	78	230	75	215		
SKOG_F_04_C	14.1	50.1	70	64	62	44		
SKOG_E_05	63.0	70.0	61	46	75	50		
SKOG_F_01	27.0	37.0	83	336	63	352		
SKOG_F_01	118.0	119.0	50	184	52	178		
SKOG_F_02	7.0	20.0	82	126	76	126		
SKOG_F_02	62.0	63.0	77	132	76	126		
SKOG_F_02	106.0	118.0	81	297	88	278		
SKOG_F_03	71.0	86.0	86	144	90	327		
SKOG_F_04	34.0	49.0	78	221	70	230		
SKOG_H_09	219.0	224.0	72	322	71	338		
TEL_H_08_C	36.4	42.1	63	336	64	345		
TEL_H_10	22.0	24.0	48	56	47	57		
TEL_H_11	52.0	53.0	65	162	40	142		
TEL_H_12	182.0	184.0	75	269	70	270		

**Fig. 7** Finally adjusted contours for RMR distribution in the open pit



between what it was possible to derive from the borehole information (underground) and the open pit surface mapping. The development of 3D distribution of RMR was an important milestone for the project, since it will help to estimate rock mass quality rating in future geometries of the open pit, which will also work as the baseline information for the calculation of SMR.

The process started with the interpolation of volume enclosing the different rock mass quality class presented in Table 4. Only five quality classes (class 2 to class 6) were relevant for this open pit since no rock mass classes with category 1 and 7 were registered during mapping. The 3D modeling continued with the process of “surface outcrop fitting”, which involved the modeling of each zone associated with every plane with low RMR zones. In this way, it was possible to assign the corresponding dip and dip direction to each plane allowing surface areas to extend as volumes into the rock mass aiming to intersect previously identified weakness zones. Figure 8 shows the general fitting of the final rock mass quality contours at the pit topography including isometric and cross-section view. Section A-A’ enables recognition of a plane that defines a low-RMR zone just behind the mine slope (and also daylighting at some benches). This joint set is comparable with the field observation of a joint system called crusher system (FS6) in the HW.

From the RMR map, it is clear that the areas that may be prone to instabilities are located in the HW. The north-eastern part is associated with the occurrence of joint planes related to FS6 in structural domain 08, whereas the south-west part is

more associated with bench-scale events. The developed RMR map was correlated and verified in the field and showed a good level of agreement. Morales et al. (2017) also identified and discussed possible failure geometries in both bench and slope scale of the mine for each structural domain. The results indicate that the possibilities for slope-scale failure geometries and bench-scale failure geometries are mainly present in the HW, while small block falls and toppling may possibly happen throughout the entire pit. This can also be seen through the low values of RMR in the model.

It is also possible to derive from the 3D RMR model that most of the low-RMR zones are distributed along the HW of the pit, especially in the upper benches of the north-western part and in the south-eastern portion. This distribution is in accordance with the behavior of the mine that has been observed in the field, as well as from registered instability events at the pit in the past.

### The SMR model

The calculation of the SMR was done in ArcMap following equations proposed by Tomás et al. (2007), also known as the continuous slope mass rating (CSMR). The CSMR was computed using an equation, which is similar to discrete SMR, but the difference lies in calculating the adjustment factors (F1, F2 and F3) depending on the joint-slope relationship. The functions showed maximum absolute difference with discrete functions lower than seven points and significantly reduced subjective interpretations. Similarly, the functions for SMR

correction factors reduce doubts about what score to assign to values near the border of the discrete classification. On the other hand, the factor F4 is same for both SMR and CSMR. The functions are defined as the following:

$$F_1 = \frac{16}{25} - \frac{3}{500} \arctan\left(\frac{1}{10}(|A|-17)\right) \tag{7}$$

Where A =

- $\alpha_j - \alpha_s$  difference of dip directions of joint and slope for planar failure.
- $\alpha_i - \alpha_s$  difference of dip directions of line of intersection and slope for wedge.
- $\alpha_j - \alpha_s - 180$  difference of dip directions of joint and slope minus 180 for toppling.

$$F_2 = \frac{9}{16} + \frac{1}{195} \arctan\left(\frac{17}{100}B-5\right) \tag{8}$$

Where B is equal to the dip ( $\beta_j$ ) of joint for planar failure and toppling, and to the dip of line of intersection for wedge failure.

$$F_3 = -30 + \frac{1}{3} \arctan(C) \tag{9}$$

$$F_3 = -13 - \frac{1}{7} \arctan(C-120) \tag{10}$$

Where C =

- $\beta_j - \beta_s$  difference of joint dipo and slope for planar failure, in Eq. 9.
- $\beta_i - \beta_s$  difference of dipo of line of intersection and slope for a wedge, in Eq. 9.
- $\beta_j + \beta_s$  sum of dip of joint and slope for toppling, in Eq. 10.

The stability classes and qualitative description proposed by Romana (1985) are also applicable to the CSMR values (Table 6).

In order to effectively calculate the SMR, five different layers of information were needed. Those layers were

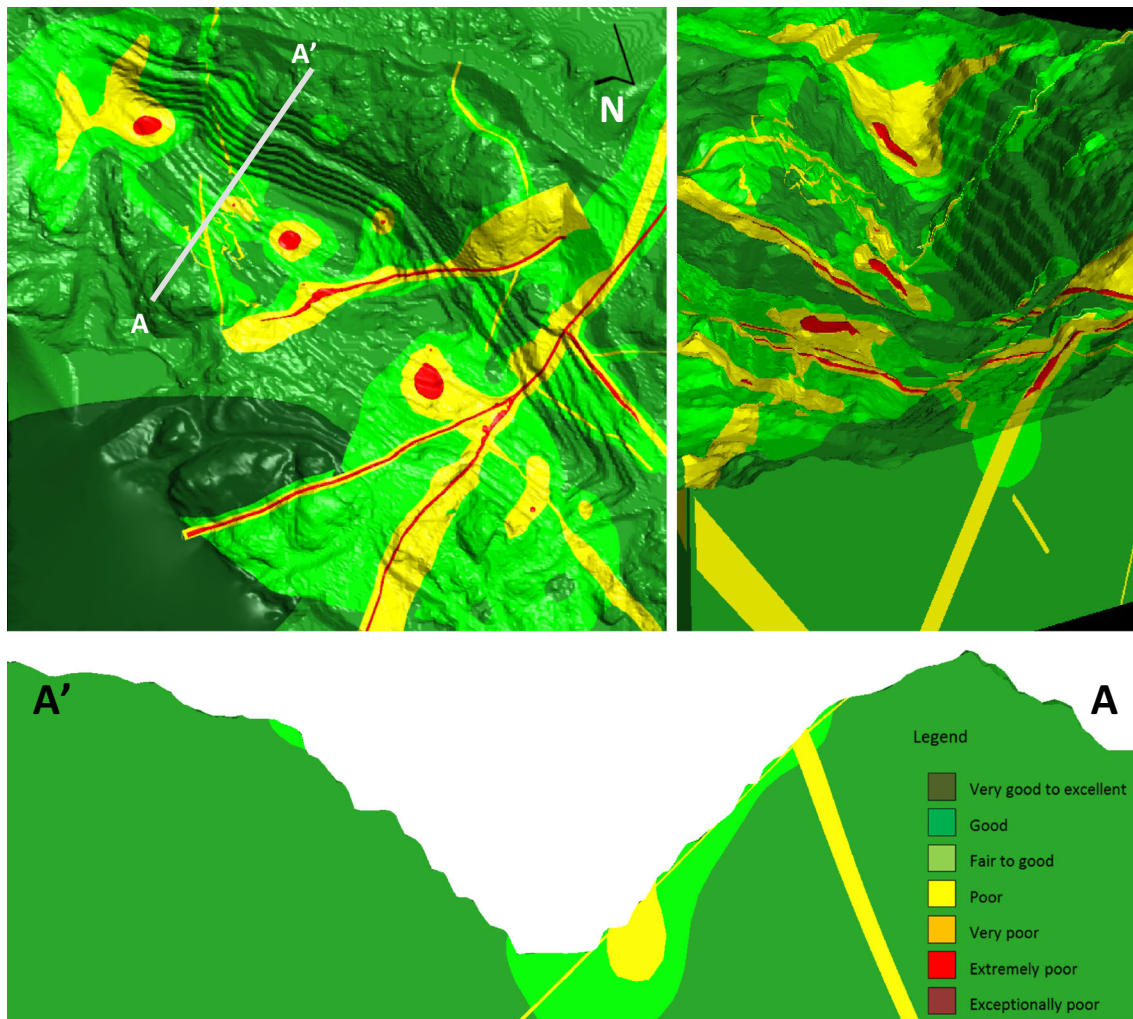


**Fig. 8** Final 3D RMR distribution. Plan view (upper left), isometric from the south east (upper right), and section A-A' (down)

**Table 6** Stability classes according to SMR values (Romana 1985)

Class	I	II	III	IV	V
SMR	81–100	61–80	41–60	21–40	0–20
Rock mass description	Very good	Good	Normal	Bad	Very bad
Stability	Completely stable	Stable	Partially stable	Unstable	Completely unstable
Failures	None	Some block failure	Planar along some joints or many wedge failure	Planar or big wedge failure	Big planar, soil-like or circular

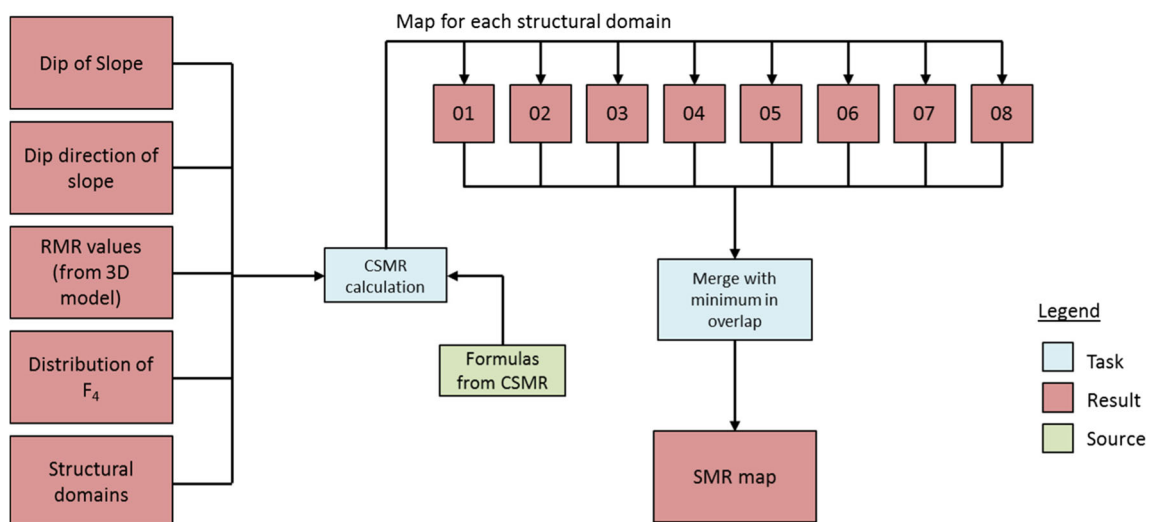
combined pixel to pixel for the calculation of a final SMR map. The necessary layers comprise: 1) dip of the slope, 2) dip direction of the slope, 3) RMR values, 4) distribution of adjustment factor for excavation method ( $F_4$ ), and 5) the structural domains that contain the information about dip and dip direction of the major joint sets. The slope layer was considered in two different ways: one layer with the overall slope angle, and the other layer with the bench face angle. Also, inside each structural domain and based on the kinematic analysis presented by Morales et al. (2017), joint sets leading to planar, wedge or toppling failure were considered. The joint sets were accounted for for an average dip and dip direction. The standard deviation of the dip and the dip direction of each joint set were considered in order to reflect the most likely directions of each joint set to assess the worst case condition.

Following this process, two resulting maps for each joint set in each structural domain were developed: 1) SMR map for the entire slope of the mine and 2) SMR map for the bench scale of the mine. If the purpose was to have just one final map, these maps might be later combined with a minimum function, in order to preserve the smaller value on each pixel. However, the authors do not recommend merging the maps since there exists the risk that SMR map may lose its meaning due to the different

scale of the problem (bench versus slope). Finally, the SMR map for each structural domain was combined to produce the final SMR map of the pit. This was accomplished by merging of the raster keeping the minimum value where overlaps were present. As seen in Fig. 1, the structural domains are overlapped. The overlapping allows better interpretation of reality, since transitions between structural domains are not strictly defined, but are most commonly seen as areas where joint sets of different structural domains coexist. A diagram illustrating the SMR calculation process is shown in Fig. 9.

A total of 16 local maps (for each of the 8 structural domains for both bench and slope scale) were produced and finally combined in order to produce two final SMR maps, as shown in Fig. 10.

From the maps it is clear to note that the possible areas that may be prone to instabilities are located in the HW in both total and bench scales. The north-eastern part is associated with the occurrence of a persisting FS (FS6) in structural domain 08, which may lead to instabilities both in bench and slope scale. On the other hand, the south-western part is most likely associated with bench-scale events, as no distinct low-SMR areas exist at the slope scale. It is emphasized here that as the mining operation at present is mainly focused in the south-western part of the pit, the overall

**Fig. 9** Detailed flowchart followed for the SMR calculation

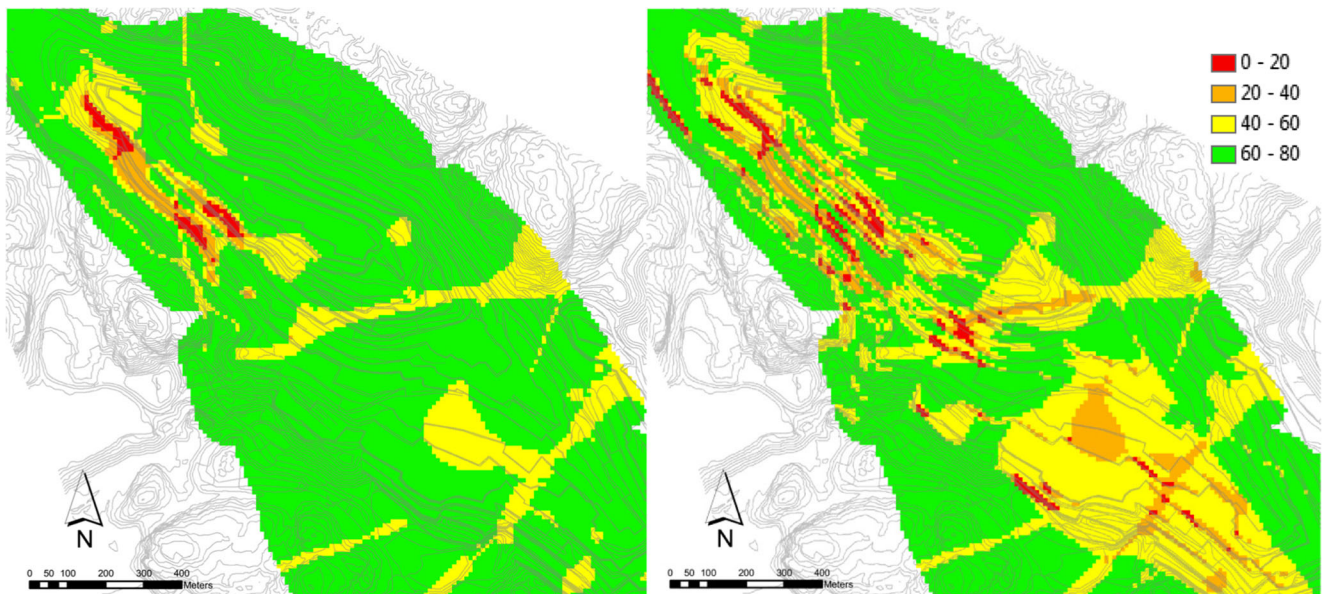


**Fig. 10** Final SMR map for the total slope (left) and for the bench slope (right)

slope angle is less than  $35^\circ$  and the topography is relatively flat at this stage of the mining.

Morales et al. (2017) identified the failure geometries at both bench and slope scale for each structural domain. The authors concluded that both slope-scale and bench-scale failure geometries are possible in the HW of the mine, while small block falls and toppling may happen throughout the pit. In this regard, the structural domains 02, 04 and 08 are the ones that possess slope-scale as well as bench-scale instabilities. This behavior is also distinguishable in Fig. 11, where the SMR map is combined with structural domains of the mine.

## Discussion

In general terms, one can conclude that the bench-scale map is able to depict the stability conditions with a good level of agreement with what is perceptible in the field. There are small inaccuracies coming from the fact that structural domains are more generalizations of average conditions within certain limits. As is recognizable, the imprecisions are found at the boundaries of the structural domains. As identified in the field, there are three zones showing lower quality than presented above, which occur mainly at the border of

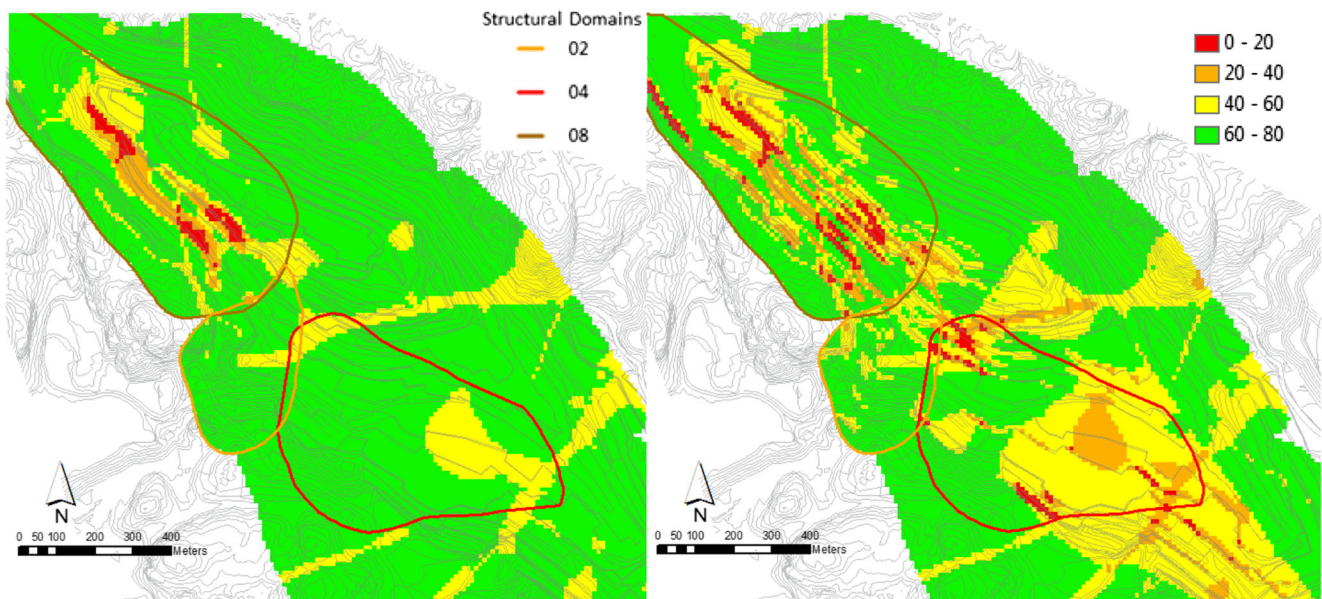


**Fig. 11** Final SMR map with structural domains for total slope (left) and for bench slope (right)

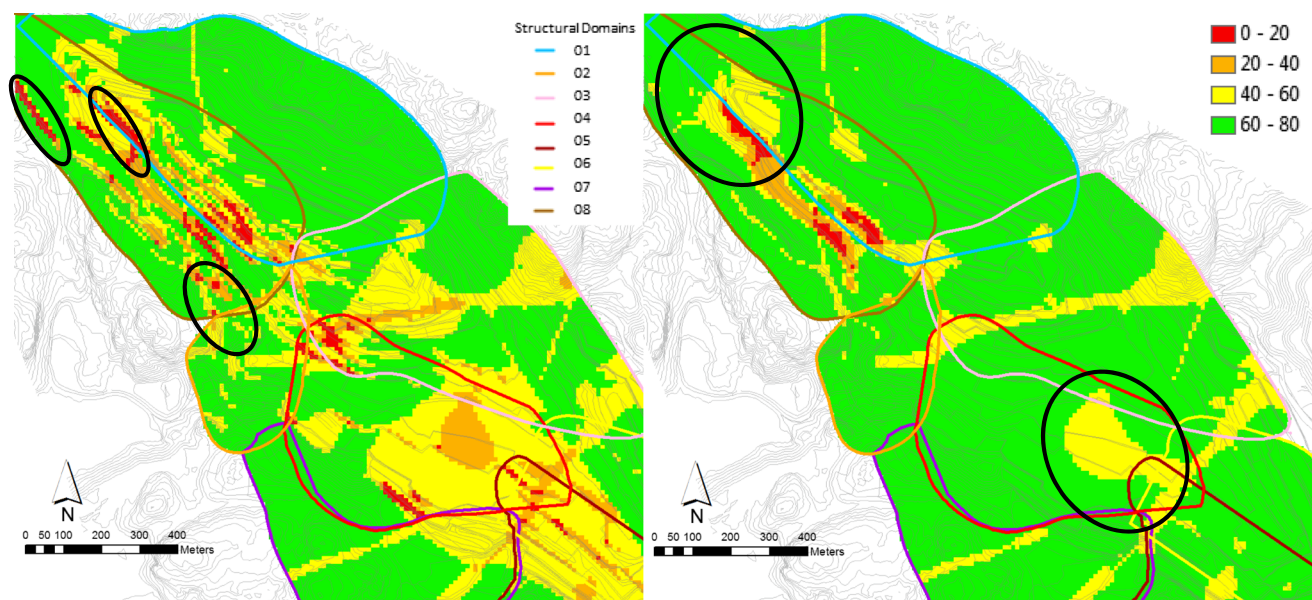


**Fig. 12** Zones with underestimated SMR quality in total slope (left) and bench slope (right)

structural domain 08 approaching structural domains 01 and 02. These inaccuracies are highlighted in Fig. 12.

On the other hand, the overall slope map is not as accurate as expected. In the south-eastern area, it fails to depict the current conditions, while in the north-western part of the pit, it gives a slightly coarse image of the areas prone to instabilities (Fig. 12). There are two reasons that explain this result:

1. When the structural domains were defined, the amount of fractures mapped on the surface was much greater than those that were taken into account from the boreholes. As a result, the 3D envelopes of the domains are more accurate close to the slope face and not as accurate when going deeper, while the influence of the information from boreholes becomes dominant. So, if we had “220 boreholes” and not only 22, then the reliability would have been much higher. The percentage of mapped joints on the surface corresponds to 77%, meaning only 23% of the information was coming from the mapping of boreholes.
2. The overall slope angle is a reinterpretation of the current topography based in the creation of new contours from a surface generated from the topography. As the distance and baseline for the new contours are decided arbitrarily, the value of SMR might be slightly different if one selects different parameters in order to create the base map.

Therefore, the SMR maps presented here should give somewhat conservative interpretation of the conditions of the slope around the mine, as highlighted by Romana et al. (2001). Similarly, it is equally important to mention here that none of the zones (both total slope and bench slope) that are currently facing unstable conditions were avoided by this analysis, i.e. the value of the SMR index has not been overestimated.

## Conclusions

The comparative study in correlating links between different rock mass classification methods has indicated fairly good agreement, as suggested by Bieniawski (1989) and Hoek (1997), which enabled further development of a 3D rock mass model of the mine. The development of the 3D rock mass model of the pit gave an overview of RMR values in space, which is useful to identify areas with low RMR all along the HW of the pit. This distribution is in agreement with the behavior of the mine that has been observed in the field, as well as from past recorded instability events. However, it is important to note that there are areas where RMR surface maps with low ratings are not always linked to potential failure modes. It is also well-known that in hard rock open pit mining, the failure modes are defined by slope geometry and orientation and their character of the discontinuities prevailing at both the total slope and the bench-scale slopes. The SMR map showed that most likely slope scale instabilities will be concentrated in the HW, while bench-scale failures may potentially appear in both the HW and in the foot wall at the south-eastern area of the mine. As demonstrated here, the SMR map provides a much enhanced picture of the stability situation of the open pit than that of the 3D RMR model. In addition, it is highlighted here that the stability assessment based on only geometrical analysis, with, for example, a joint set dipping at  $82^\circ$  and having direction parallel to the bench face dipping at  $85^\circ$  fulfills the criteria of a plane failure, may not necessarily mean that the slope will fail since the failure will depend on the frictional properties of the most vulnerable discontinuity set in question.

This research has also demonstrated that calculating SMR surface values from a 3D RMR model is a very fruitful

methodology not only for assessing present events, but also for assessing potential future instability events, since this can be easily seen by developing future topographic condition of the mine for short-, medium- and long-term mine operation. Moreover, the 3D RMR model may be used to predict rock mass conditions by intersecting the domains with future pit topographies, and later to calculate the SMR in order to depict future stability conditions. The presented methodology can be replicated in any other open pit mine with a similar level of geotechnical information. Hence, the development of a 3D picture of the rock mass should be incorporated as a part of the mine plan so that all short-, medium- and long-term challenges are visualized and appropriate measures are in place to avoid serious and significant future instabilities.

## References

- Aksoy CO (2008) Review of rock mass rating classification: historical developments, applications, and restrictions. *J Min Sci* 44(1):51–63
- Barton N, Choubey v (1977) The shear strength of rock joints in theory and practice. *Rock Mech* 10(1):1–54. <https://doi.org/10.1007/BF01261801>
- Barton NR, Lien R, Lunde J (1974) Engineering classification of rock masses for the design of tunnel support. *Rock Mech* vol 6(4):189–239
- Bieniawski ZT (1973) Engineering classification of jointed rock masses. *Trans South African Institute of Civil Engineering*, vol 15:335–344
- Bieniawski ZT (1989) Engineering rock mass classifications: A complete manual for engineers and geologists in mining, civil, and petroleum engineering. New York: Wiley
- Chilès JP (1988) Fractal and geostatistical method for modelling a fracture network. *Math Geol* 20(6):631–654
- Choi Y, Yoon SY, Park HD (2009) Tunneling analyst: a 3D GIS extension for rock mass classification and fault zone analysis in tunneling. *Comput Geosci*, vol 35:1322–1333
- Egaña M, Ortiz J (2013) Assessment of rmr and its uncertainty by using geostatistical simulation in a mining project. *J GeoEng* 8(3):83–90
- Ellefmno SL, Eidsvik J (2009) Local and spatial joint frequency uncertainty and its application to rock mass characterisation. *Rock Mech Rock Eng* 42(4):667–688
- Exadaktylos G, Stavropoulou M (2008) A specific upscaling theory of rock mass parameters exhibiting spatial variability: analytical relations and computational scheme. *Int Journal Rock Mech Min Sci* 45:1102–1125
- Exadaktylos G, Stavropoulou M, Xiroudakis G, de Broissia M, Schwarz H (2008) A spatial estimation model for continuous rock mass characterization from the specific energy of a TBM. *Rock Mech Rock Eng* 41:797–834
- Ferrari F, Apuani T, Giani GP (2014) Rock mass rating spatial estimation by geostatistical analysis. *International Journal of Rock Mechanics & Mining Sciences* 70:162–176
- Flores G, Karzulovic A (2002) Geotechnical guidelines for a transition from open pit to underground mining. Benchmark report. Project ICS-II, task 4
- Hoek E (1994) Strength of rock and rock masses. *News J ISRM* 2(2):4–16
- Hoek E (1997) Practical estimates of rock mass strength. *Int J Rock Mech Min Sci* 34(8):1165–1186
- Hoek E (2006) Practical rock engineering. e-notes available at Hoek's corner. [www.rocscience.com](http://www.rocscience.com)
- Laubscher DH (1990) A Geomechanics classification system for the rating of rock mass in mine design. *JS Afr Inst Mining Metallurgy* 90(86):257–273
- Long JCS, Billiaux DM (1987) From field data to fracture network modeling: an example incorporating spatial structure. *Water Resour Res* 23(7):1201–1216
- Marinos P, Hoek E (2000) GSI: a geologically friendly tool for rock mass strength estimation. In: *Proceedings of the GeoEng2000 at the international conference on geotechnical and geological engineering*, Melbourne. Technomic publishers, Lancaster, pp 1422–1446
- Marinos V, Marinos P, Hoek E (2005) The geological strength index: applications and limitations. *Bull Eng Geol Environ* 64:55–65
- Morales M, Panthi KK, Botsialas K, Holmøy KH (2017) Development of a 3D structural model of a mine by consolidating different data sources. *Bull Eng Geol Environ*. <http://dx.doi.org/10.1007/s10064-017-1068-6>
- Öztürk CA (2002) Geostatistical assessment of rock zones for tunneling. *Tunneling and Underground Space Technology* 17:275–285
- Palmstrom A, Broch E (2006) Use and misuse of rock mass classification systems with particular reference to the Q-system. *Tunnels and Underground Space Technology* 21:575–593
- Pantelidis L (2009) Rock slope stability assessment through rock mass classification systems. *International Journal Rock Mech Min Sci* 46(2):315–325
- Panthi KK (2006) Analysis of engineering geological uncertainties related to tunneling in Himalayan rock mass conditions. Doctoral thesis, Norwegian University of Science and Technology, ISBN 82–471–7826-5
- Panthi KK, Nilsen B (2006) Numerical analysis of stresses and displacements for the Tafjord slide, Norway. *Bull Eng Geol Env*, vol 65:57–63
- Rafiee A, Vinches M (2008) Application of geostatistical characteristics of rock mass fracture system in 3D model generation. *International Journal Rock Mech Min Sci* 45:644–652
- Read J, Stacey P (2009). *Guidelines for Open Pit Slope Design*. ISBN: 9780643094697, pp 69–82
- Riglar B, Botsialas K, Morales M (2016). Structural characterization of hard rock formation using wireline borehole logging techniques in an open pit mine, Norway. *Proceedings of the 17th Nordic Geotechnical Meeting, NGM Reykjavik 2016*, pp 1203–1212
- Romana M (1985) New adjustment ratings for application of bieniawski classification to slopes. *Proceedings of International Symposium on the Role of Rock Mechanics, ISRM, Salzburg*, pp. 49–53
- Romana M (1993) A geomechanical classification for slopes: slope mass rating. *Comprehensive rock engineering*, John A. Hudson, Editor-in-Chief. Oxford: Pergamon 3: pp 1–45
- Romana M, Serón JB, Montalnar E (2001). La clasificación geomecánica SMR: aplicación experiencias y validación. In *proceedings of V Simposio Nacional sobre Talues y Laderas inestables*. Madrid, pp.393–404
- Ryu DW, Kim TK, Heo JS (2003) A study on geostatistical simulation technique for the uncertainty modeling of RMR. *Tunnel and Underground* 13:87–99
- Stavropoulou M, Exadaktylos G, Saratsis G (2007) A combined three-dimensional geological-geostatistical-numerical model of underground excavations in rock. *Rock Mech Rock Eng* 40(3):213–243
- Steffen OKH, Holt W, Symons VR (1970) Optimizing open pit geometry and operational procedure. In *Planning Open Pit Mines, Proc Symposium on the Theoretical Background to the Planning of Open Pit Mines with Special Reference to Slope Stability*. Johannesburg, August 29–September 4, 1970, pp. 9–31
- Tomás R, Delgado J, Serón JB (2007) Modification of slope mass rating (SMR) by continuous functions. *Int J Rock Mech Min Sci* 44:1062–1069
- You K, Lee JS (2006) Estimation of rock mass classes using the 3-dimensional multiple indicator kriging technique. *Tunn Undergr Space Technol* 21(3–4):229
- Yu YF, Mostyn GR (1993) *Spatial correlation of rock joints*. Probabilistic methods in geotechnical engineering. Balkema, Rotterdam